Nanoscale

PAPER

Cite this: *Nanoscale*, 2015, **7**, 3173

Highly efficient quantum dot-sensitized TiO_2 solar cells based on multilayered semiconductors (ZnSe/CdS/CdSe)†

Lin Yang,[a,b] Connor McCue,[c] Qifeng Zhang,[b] Evan Uchaker,[b] Yaohua Mai[a] and Guozhong Cao*[b,d]

Received 23rd November 2014,
Accepted 29th December 2014

DOI: 10.1039/c4nr06935h

www.rsc.org/nanoscale

A new approach by inserting a layer of ZnSe QDs was studied to enhance the adsorption of CdS/CdSe QDs resulting in much improved power conversion efficiency. ZnSe, CdS and CdSe QDs were sequentially assembled on a nanocrystalline TiO_2 film to prepare a ZnSe/CdS/CdSe sensitized photoelectrode for QD-sensitized solar cell (QDSSC) applications. The results show that the performance of QDSSCs is strongly dependent on the order of the QDs with respect to TiO_2. The pre-assembled ZnSe QD layer acts as a seed layer in the subsequent SILAR process, inducing both the nucleation and growth of CdS QDs, whereas CdS and CdSe QDs have a complementary effect in light harvesting. In the cascade structure of TiO_2/ZnSe/CdS/CdSe electrode, a high efficiency of 4.94% and a long electron lifetime of 87.4 ms were achieved, which can be attributed to the following factors: the higher intensity and red shift of light absorption in 400–700 nm range increase the electron concentration in TiO_2 substrate sensitized by ZnSe/CdS/CdSe compared to the others, which directly accelerate electron transport in TiO_2 and their transfer to FTO glass; the re-organization of energy levels among ZnSe, CdS and CdSe forms a stepwise structure of band-edge levels, which is advantageous to the electron injection and hole recovery of QDs.

Introduction

Dye-sensitized solar cells (DSSCs) have received considerable attention over the past few decades because of their high efficiency and relatively inexpensive fabrication process compared with the conventional inorganic solar cells.[1–3] DSSCs are based on the photosensitization of nanocrystalline TiO_2 photoelectrodes by absorbed dyes. One of the key factors determining the efficiency of DSSC is light-harvesting.[4,5] Recently, there has been significant interest in solar cells based on perovskite absorbers,[6,7] which enable complete light absorption in considerably thinner films. However, perovskite solar cells suffer from moisture-sensitive nature. Therefore, semiconductor quantum dots (QDs), which have extraordinary optical and electrical properties, can be viable alternatives to ruthenium complexes or organic dyes in sensitized solar cell applications. There are some specific advantages of using semiconductor QDs as the light absorbers. Owing to the quantum confinement effect, the optical properties of QDs can be adjusted by changing their size, and it is possible to generate multiple electron–hole pairs per photon through the impact ionization effect. Another advantage of QD sensitizers over conventional dyes is their high extinction coefficient,[8,9] which is known to reduce the dark current and increase the overall efficiency of the solar cells.

Considerable studies related to QD sensitizers have been performed on narrow band gap semiconductor QDs including CdS,[10,11] CdSe,[12,13] CdTe,[14] PbS,[15,16] PbSe,[17] and InP.[18] Among these QDs, CdS and CdSe are more promising materials that have been reported to exhibit better performance. In particular, the multilayered semiconductor QD-sensitizers including CdSe QDs with inner CdS layer and/or outer ZnS layers showed impressive results, comparable to those of DSSCs, when assembled to a solar cell, and then tested with polysulfide electrolytes; thus, they are being considered as an important system in QD-sensitized solar cells (QDSSCs). On the basis of a TiO_2 nanotube, Gao *et al.*[19] prepared a CdS/CdSe co-sensitized solar cell with a short circuit current density of 13.0 mA cm^{-2}. Lee and Lo[20] prepared a TiO_2/CdS/CdSe/ZnS electrode, which offers a relatively high power conversion efficiency (PCE) of

[a]*College of Physics Science and Engineering, Hebei University, Baoding 071002, Hebei, P. R. China*
[b]*Department of Materials Science and Engineering, University of Washington, Seattle, Washington 98195-2120, USA. E-mail: gzcao@u.washington.edu; Fax: +1-206-543-3100; Tel: +1-206-616-9084*
[c]*Department of Chemistry, University of Washington, Seattle, Washington 98195-2120, USA*
[d]*Beijing Institute of Nanoenergy and Nanosystems, Chinese Academy of Sciences, Beijing 100083, P. R. China*
†Electronic supplementary information (ESI) available. See DOI: 10.1039/c4nr06935h

4.22%. Lee and co-workers[21] reported a PCE of 3.44% for an electrochemical cell using a CdS/CdSe/ZnS multilayered QD-sensitized TiO_2 photoelectrode. A PCE of as high as 4.62% has been achieved by our group for CdS/CdSe co-sensitized solar cells by adjusting the thickness of the TiO_2 film.[22] Our previous work on a TiO_2 photoelectrode sensitized by $Zn_xCd_{1-x}Se$ QDs with a controlled composition gradient through an ion-exchange method indicated that effective band alignment is favorable for the performance of solar cells.[23]

In this study, multilayered semiconductor (ZnSe/CdS/CdSe) QDs were prepared on the surface of TiO_2 mesoporous films as a promising sensitizer by employing a series of successive ionic layer adsorption and reaction (SILAR) processes, which allow each layer to successively grow in a reproducible and controllable manner. The multilayered QD-sensitized solar cells yielding large short circuit currents and high efficiency are considered as an interesting alternative for QDSSCs. The cascade structure of the TiO_2/ZnSe/CdS/CdSe photoelectrode not only has a complementary effect in light harvesting, but also demonstrates efficient charge transport for both electrons and holes. Thus, it was found that by controlling the incorporation of QDs layers with the optimum deposition order and number of SILAR cycles the performance of solar cells can be enhanced.

Experimental

Chemicals and materials

Zinc acetate dihydrate ($Zn(AC)_2{\cdot}2H_2O$, AR, 98.0%), cadmium acetate dihydrate ($Cd(AC)_2{\cdot}2H_2O$, AR, 98.0%), sodium sulfide (Na_2S, AR, 98.0%), sodium borohydride ($NaBH_4$, AR, 98.0%), selenium powder (Se, −200 mesh, 3 N, 99.9%), and sulfur (S, Reagent grade) were directly used without further purification. Ultrapure deionized water was used for the preparation of all aqueous solutions.

Growth of multilayered semiconductor QDs (ZnSe/CdS/CdSe, ZnSe/CdS, ZnSe/CdSe and CdS/CdSe) by SILAR processe

An optimized mesoporous TiO_2 film (~12 μm thick) was prepared by the doctor blade-printing of a commercial TiO_2 paste (Degussa P25) onto cleaned F-doped SnO_2 (FTO) glass after being diluted with pure ethanol, and the sintering temperature was gradually increased to 500 °C and maintained for 30 min to improve the crystallinity and remove impurities. An aqueous solution of Se source (NaHSe) was first prepared by mixing sodium borohydride ($NaBH_4$) and selenium powder in deionized water with vigorous stirring while the container was purged with N_2. TiO_2 films were successively immersed into two different aqueous solutions for 2 min each, first in 0.06 M $Zn(AC)_2$ and then in 0.06 M NaHSe. Following each immersion, the films were rinsed with deionized water to remove excess precursors and dried before the subsequent dipping. This immersion cycle was repeated ten times for the ZnSe layer (designated as ZnSe(10)). For CdS deposition, aqueous solutions of 0.06 M $Cd(AC)_2$ and 0.06 M Na_2S were used for five successive SILAR cycles with a dipping time of 2 min each (CdS(5)). For CdSe deposition, aqueous solutions of 0.06 M $Cd(AC)_2$ and 0.06 M NaHSe were used for eight successive SILAR processes with a dipping time of 2 min each (CdSe(8)). For CdS monolayer, ZnSe/CdS, ZnSe/CdSe and CdS/CdSe multilayer coating, the same procedure described above was used over the TiO_2 electrode.

Electrolyte solution and counter electrode for QDSSC fabrication

The polysulfide electrolyte solution was freshly prepared prior to each measurement by dissolving 1 M Na_2S and 1 M S in deionized water. Nanostructured Cu_2S counter-electrodes were prepared by immersing a brass sheet in a HCl solution (37 wt%) at 80 °C for 40 min and subsequently dipping it into the fresh prepared polysulfide electrolyte for 5 minutes. The counter electrode and a QD-sensitized photoelectrode were assembled into a sandwich-type configuration using a Scotch spacer (thickness of 50 μm) and with a droplet (10 μL) of polysulfide electrolyte.

Characterization

Transmission electron microscopy (TEM) was carried out on a Tecnai G2 F20 TEM. The film was scratched off the FTO glass and ultrasonically dispersed in ethanol. Subsequently, a few drops of the resulting dispersion were placed on a grid for TEM observation. Energy dispersion X-ray (EDX) and elemental mapping on the samples was carried out by EDX integrated in SEM (JSM-7000). The optical properties of the samples were characterized by UV-vis spectrophotometry (Perkin Elmer Lambda 900). The photocurrent–voltage (I–V) curves were recorded on a Keithley 2400 Sourcemeter under the illumination of an AM 1.5 solar simulator (100 mW cm^{-2}, HP 4155A, equipped with a 500 W xenon arc lamp). Electrochemical impedance spectroscopy (EIS) was performed on a Solartron 1287A, coupled with a Solartron 1260 FRA/impedance analyzer in the dark by applying a bias voltage of −0.6 V from 10^{-1} to 10^5 Hz to investigate the charge dynamics of the QDSSCs.

Results and discussion

A typical high-resolution TEM image (Fig. 1) was obtained to characterize the arrangement of QDs on the internal surface of mesoporous TiO_2 film. Various crystalline planes are clearly observed. The larger crystallite appearing in the left region of Fig. 1 is identified to be TiO_2. The measured lattice spacing of this crystalline plane is 0.352 nm, corresponding to the (101) plane of anatase TiO_2 (JCPDS 21-1272).[24] Around the TiO_2 crystallite, well-crystallized QDs with various orientations and lattice spacings are observed. A careful inspection and comparison of the lattice parameters also indicate that the QDs connected to the TiO_2 are ZnSe, and CdSe QDs are located outside the CdS. The lattice spacings of 0.327, 0.338 and 0.351 nm in the polycrystalline particle are matching well to the interplanar spacing of the (111) planes of cubic

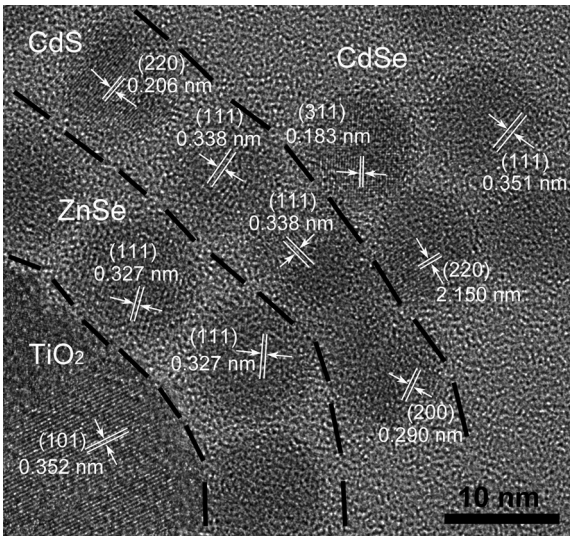

Fig. 1 High-resolution TEM image showing the arrangement of ZnSe/CdS/CdSe QDs around a TiO_2 crystallite.

ZnSe, CdS and CdSe QDs, respectively. Therefore, the cascade structure of ZnSe/CdS/CdSe assembled on the TiO_2 surface is confirmed by HRTEM. Moreover, the size range of the QDs is found to be 8–10 nm, which is consistent with the crystal sizes evaluated from the UV-vis spectra.

The compositional EDX analysis was carried out on TiO_2/ZnSe/CdS/CdSe electrode. With regard to the EDX spectra, shown in Fig. 2a, the atomic ratio of Zn : Cd : S : Se is calculated to be about 42.6 : 77.4 : 28.1 : 91.7 for TiO_2/ZnSe/CdS/CdSe, which suggests that the QDs consist of ZnSe, CdS and CdSe with a molar ratio of 35.5 : 23.5 : 41.0 (calculation in the ESI†). As illustrated in Fig. 2b, the corresponding Cd, Se, Zn, and S EDX elemental maps show that these elements are homogeneously distributed throughout the films.

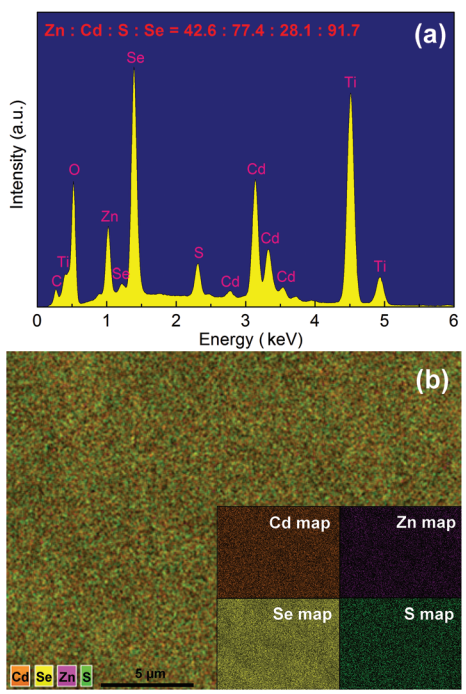

Fig. 2 (a) EDX spectra of TiO_2/ZnSe/CdS/CdSe electrode; (b) element distribution maps of Cd, Zn, Se and S.

The amount of CdS incorporated in the TiO_2 film was evaluated using the UV-vis absorption spectra. Fig. 3 shows the variation of the spectra with the SILAR cycles. For the process performed on the bare TiO_2 film (Fig. 3a), the amount of CdS QDs incorporated is small, as indicated by the lower absorbance of the TiO_2/CdS electrodes and the observation of a color change in the film. The absorbance slowly increases with increasing number of cycles, along with a slight red shift of the absorption shoulder. In the presence of a ZnSe QDs seed layer, the amount of CdS incorporated is greatly enhanced, as demonstrated by the higher absorbance, especially in the early SILAR cycle, as shown in Fig. 3b. The larger red shift of the absorption shoulder with increasing number of cycles implies the growth of CdS QDs. It is noteworthy that the absorbance of the CdS assembled in the presence of ZnSe after five cycles is almost double of that assembled in the absence of ZnSe. These results demonstrate the growth enhancement effect of the seed layer on the deposition of CdS. Herein, it could be concluded that the ZnSe layer favors the nucleation and growth of CdS, leading to a high deposition rate of CdS in the SILAR process. In addition, there is an optimal amount of QDs incorporated in the TiO_2/ZnSe/CdS systems. After a careful study on the effects of the number of SILAR cycles on the device performance, the optimum numbers of cycles for incorporating ZnSe and CdS QDs in the present study are found to be around 10 and 5, respectively.

When a subsequent SILAR process was performed to deposit CdSe QDs on the TiO_2/ZnSe/CdS electrode, the resulting UV-vis spectra in Fig. 4 show an increase in the absorbance with increasing SILAR cycle, as well as the red shifts of the absorption shoulder and onset position. These results indicate that more CdSe QDs are deposited on the TiO_2 matrix during the SILAR process and the size of CdSe QDs increases after each SILAR cycle. For the TiO_2/ZnSe/CdS electrode containing only a one cycle-deposited CdSe QDs layer, the absorption edge obtained from the intersection of the baseline with the tangent line of the sharply decreasing region of the spectrum is approximately 595 nm, corresponding to a band gap of 2.08 eV. Using the Brus equation, the size of CdSe QDs estimated from the band gap is 5.82 nm. For TiO_2/ZnSe(10)/CdS(5)/CdSe(6) photoelectrode, the mean size of CdSe QDs estimated from the band gap (679 nm, 1.83 eV) is 10.03 nm, which is close to the value obtained from TEM (Fig. 1). Thus, the growth rate of the SILAR process is ~0.84 nm per cycle.

The inset in Fig. 4 shows the absorbance after various cycles of the SILAR process. With increasing number of SILAR cycles, the absorbance moderately increases in the early cycles and then the increase gradually slows, approaching a constant value after six to eight cycles. The higher increment of absorbance in the early cycles is attributed to the higher

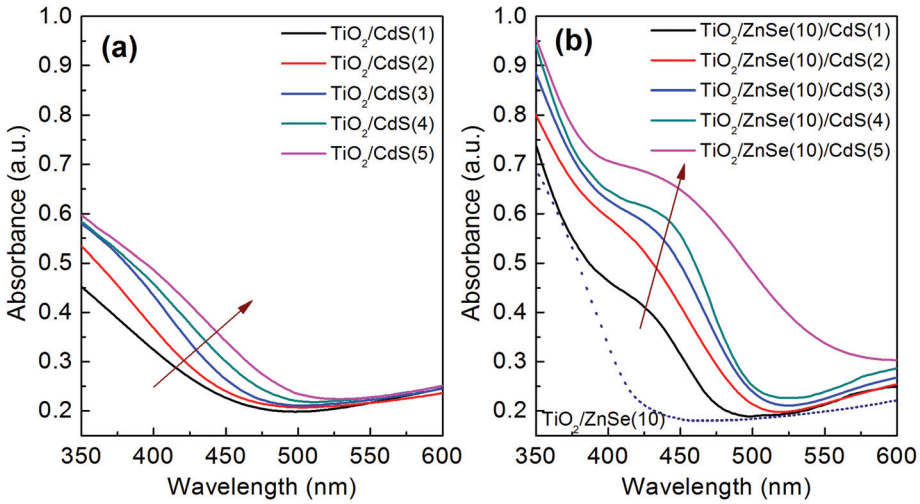

Fig. 3 UV-vis absorption spectra of CdS QD-sensitized TiO_2 films prepared from various cycles of the SILAR process in the absence (a) and in the presence (b) of a layer of ZnSe QDs. The number after the designated semiconductor QDs indicates the number of SILAR cycles.

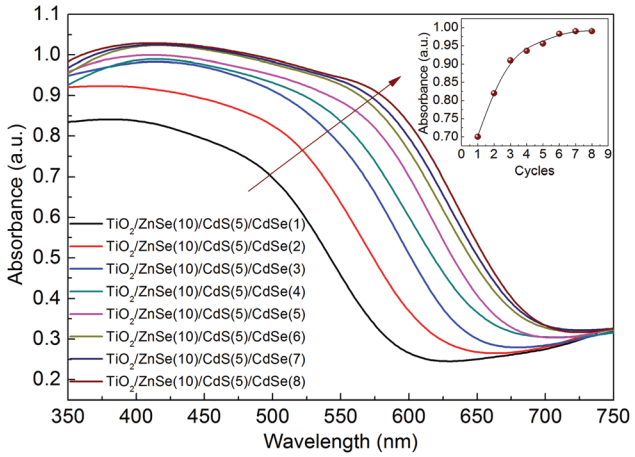

Fig. 4 UV-vis absorption spectra of TiO_2/ZnSe/CdS/CdSe photoelectrode prepared from various SILAR cycles for assembling CdSe layer. The inset shows the dependence of absorbance (in the wavelength of 500 nm) on the number of SILAR cycles.

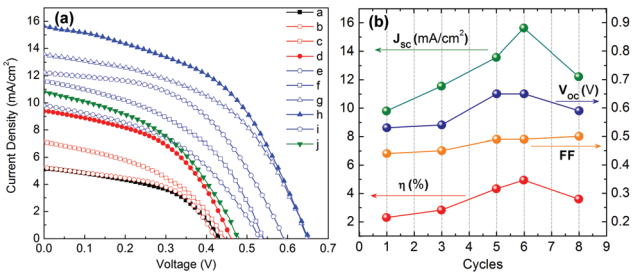

Fig. 5 (a) Current density–voltage (I–V) characteristics of QDSSCs using various multilayered QD-sensitized TiO_2 photoelectrode; (b) dependence of photovoltaic parameters on the number of SILAR cycles for the QDSSCs using TiO_2/ZnSe/CdS/CdSe as photoelectrode.

surface area of the mesoporous TiO_2 matrix available for adsorption, which would be blocked after six cycles making the additional deposition of QDs difficult. In addition, when CdSe QDs were assembled on the TiO_2/ZnSe electrode, the photoelectrode TiO_2/ZnSe/CdSe has an absorption edge close to that of TiO_2/ZnSe/CdS/CdSe, but its absorbance is lower than the latter, as shown in Fig. S1a (ESI†), particularly in the short wavelength region (<550 nm), where both CdS and CdSe QDs are photoactive.[19] Thus, the higher absorbance of TiO_2/ZnSe/CdS/CdSe can be attributed to the co-absorption of sunlight in the two materials. The presence of CdS QDs has an appreciable impact on light harvesting, contributing to the performance of solar cells. It is worth noting that the absorbance of TiO_2/CdS/CdSe is considerably lower than that of TiO_2/ZnSe/CdS/CdSe, even though they have a similar absorption edge (Fig. S1b†), which is generally ascribed to the smaller amount of CdS QDs incorporated in the absence of a ZnSe layer, which provides further evidence of the effect of a ZnSe seed layer.

Fig. 5a shows the current density–voltage (I–V) characteristics of the solar cells configured using the samples as the photoanodes, a Cu_2S as the counter electrode, and an aqueous solution of 1 M Na_2S and 1 M S as the electrolyte. Key performance parameters of various cells are summarized in Table 1. When only a layer of CdS was present on the bare TiO_2 film, the device generates a short circuit current density (J_{SC}) of 5.15 mA cm^{-2}, an open circuit voltage (V_{OC}) of 0.44 V, and a fill factor (FF) of 0.48, yielding a very low power conversion efficiency (η) of 1.09%. However, when a layer of ZnSe was introduced, both J_{SC} and η slightly increase with increasing number of SILAR cycles for CdS, while their V_{OC} remained at ~0.44 V. Consequently, the small J_{SC} and FF for TiO_2/CdS provide further evidence that only a small amount of CdS QDs has been incorporated into the bare TiO_2 film,[25] which also implies that the ZnSe seed layer contributes to the performance enhancement in the subsequent photoanodes.

Table 1 Photovoltaic parameters obtained from the *I–V* curves of QDSSCs using various photoanodes

No.	Photoanode	V_{oc} (V)	J_{sc} (mA cm^{-2})	FF	Efficiency (%)
a	TiO_2/CdS(5)	0.44	5.15	0.48	1.09
b	TiO_2/ZnSe(10)/CdS(1)	0.42	5.23	0.52	1.14
c	TiO_2/ZnSe(10)/CdS(3)	0.44	7.11	0.42	1.35
d	TiO_2/ZnSe(10)/CdS(5)	0.46	9.37	0.48	2.07
e	TiO_2/ZnSe(10)/CdS(5)/CdSe(1)	0.53	9.80	0.44	2.30
f	TiO_2/ZnSe(10)/CdS(5)/CdSe(3)	0.54	11.56	0.45	2.83
g	TiO_2/ZnSe(10)/CdS(5)/CdSe(5)	0.65	13.58	0.49	4.33
h	TiO_2/ZnSe(10)/CdS(5)/CdSe(6)	0.65	15.64	0.49	4.94
i	TiO_2/ZnSe(10)/CdS(5)/CdSe(8)	0.59	12.22	0.50	3.60
j	TiO_2/CdS(5)/CdSe(6)	0.48	10.79	0.44	2.26

For TiO_2/ZnSe/CdS/CdSe electrode, with the increasing number of SILAR cycles for assembling CdSe layer, both J_{SC} and V_{OC} drastically increase from 9.80 mA cm^{-2} and 0.53 V for one cycle (curve e in Fig. 5a) to 11.56 mA cm^{-2} and 0.54 V for three cycles (curve f), and 15.64 mA cm^{-2} and 0.65 V for the six cycles (curve h), respectively, as clearly demonstrated in Fig. 5b. η increases with the increasing number of SILAR cycles, reaching a maximum value of 4.94% at six cycles, and then decreases with a further increase in the number of cycles. In the SILAR process, the deposited amount and crystal size of CdSe QDs concomitantly increase with the increasing number of SILAR cycles. The larger amount of CdSe QDs deposited increases the light absorption. However, increase in the crystal size would decrease the driving force for interfacial electron transfer due to the lower conduction band or less quantum confinement, whereas charge recombination can be suppressed.[9] In the present case, the early cycles are supposed to increase the coverage ratio of CdSe on the TiO_2 surface by replenishing the uncovered area left by the SILAR process. Furthermore, the thickness of the CdSe layer would increase after each cycle. Such an increase in the deposited CdSe QDs leads to much more excited electrons under light illumination, which is advantageous to the photocurrent of QDSSCs. However, the contacting area of QDs/electrolyte will decrease with increasing number of SILAR cycles because more pores are probably blocked by the additional CdSe QD loading. This also suggests that as the layer thickness continuously increases, it will be more difficult to inject an excited electron generated in the outer layer into the TiO_2 matrix due to the increased charge recombination in QDs. The competition between these effects determines the optimal number of SILAR cycles (6) to be performed to deposit the CdSe QDs. In addition, the efficiency of QDSSCs based on the TiO_2/ZnSe(10)/CdS(5)/CdSe(6) photoelectrode is maintained at a high value, which slightly decreases (<10%) after several days, indicating their good stability under ambient conditions (shown in Fig. S2†).

Fig. 6a shows the EIS results containing typically two semicircles, which are fitted by an equivalent circuit (inset in Fig. 6a) with the fitted values listed in Table 2. R_S is the substrate resistance. R_1 and CPE_1 represent the charge transfer resistance and capacitance at counter electrode/electrolyte interface, respectively, while R_2 and CPE_2 represent the recombination resistance and capacitance at the photoanode/electrolyte interface, respectively.[26] At the counter electrode/electrolyte interface, the recombination resistance, R_1, exhibits no apparent differences among these three QDSSCs while the same counter electrode and electrolyte are used in these experiments. The simulated data of charge transfer resistance R_2 for the electron transfer process at TiO_2/ZnSe/CdS/CdSe QDs/electrolyte interface is higher than that of the QDSSCs with the other layers due to the reduced interfacial recombination.

Table 2 Simulated values of resistance (*R*), capacitance (CPE) and electron lifetime (τ_n) of the EIS spectra calculated by an equivalent circuit

Photoanode	R_S (Ω)	R_1 (Ω)	CPE_1 (μF)	R_2 (Ω)	CPE_2 (μF)	τ_n (ms)
TiO_2/CdS(5)	11.66	2.65	175	27.88	348	9.7
TiO_2/ZnSe(10)/CdS(5)	12.01	2.73	155	117.34	418	49.1
TiO_2/ZnSe(10)/CdS(5)/CdSe(3)	11.05	2.81	106	188.62	406	76.5
TiO_2/ZnSe(10)/CdS(5)/CdSe(6)	10.91	2.88	137	250.91	348	87.4
TiO_2/ZnSe(10)/CdS(5)/CdSe(8)	9.20	2.90	98	171.72	351	60.3

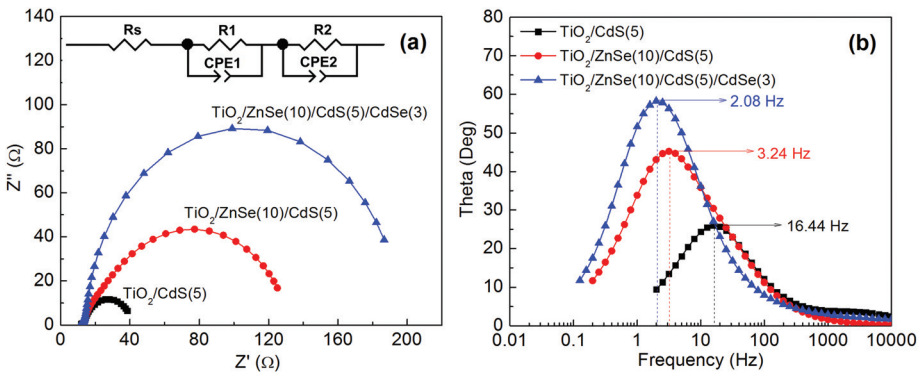

Fig. 6 Nyquist curves (a) and Bode plot curves (b) of QDSSCs based on different layered QD-sensitized TiO_2 photoanode measured in the dark at −0.6 V bias. The inset in (a) illustrates the equivalent circuit simulated to fit the impedance spectra.

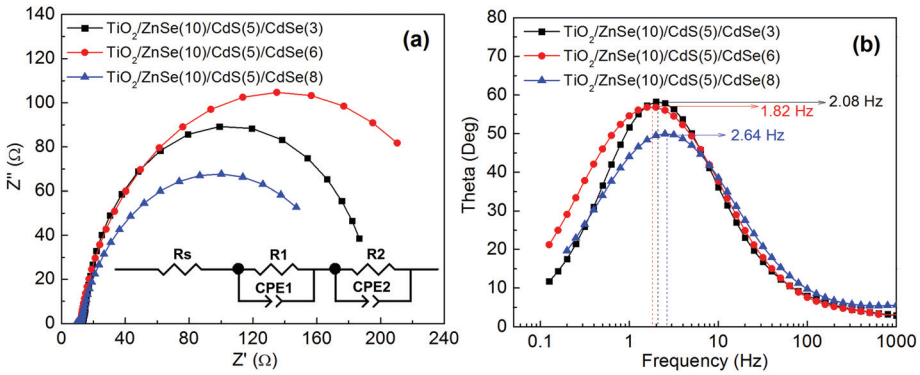

Fig. 7 Nyquist curves (a) and Bode plot curves (b) of QDSSCs based on TiO_2/ZnSe/CdS/CdSe photoanode measured in the dark at −0.6 V bias. The inset in (a) illustrates the equivalent circuit simulated to fit the impedance spectra.

The electron lifetimes (τ_n) in photoanodes can be evaluated by $\tau_n = R_2 \times CPE_2$.[26,27]

According to Table 2, the τ_n for TiO_2/CdS (9.7 ms) is considerably shorter than that for TiO_2/ZnSe/CdS (49.1 ms) and TiO_2/ZnSe/CdS/CdSe (≥76.5 ms). Fig. 7 shows the EIS results of the QDSSCs based on TiO_2/ZnSe/CdS/CdSe photoanode with the fitted values listed in Table 2. In the present case, TiO_2/ZnSe(10)/CdS(5)/CdSe(6) is suggested to show the largest R_2, contributing to obvious improvement in J_{SC} and FF.[28] This indicates that τ_n can be maintained at the high value, ~87.4 ms at six cycles. The long-lived charge carrier implies low charge recombination to improve V_{oc}. However, the electron lifetime drops to ~60.3 ms when eight SILAR cycles are applied.

According to the data reported in the literature,[29–31] the band edges and relative Fermi levels positions of TiO_2, ZnSe, CdS, and CdSe in the bulk are schematically shown in Fig. 8a. TiO_2 is typically an n-type semiconductor,[32] and it is possible that ZnSe and CdS QDs become n-type, in which the electrons are the mobile charge carriers in photoelectrochemical cells. When TiO_2, ZnSe, CdS and CdSe are connected together, the difference in energy levels induces electron flow from the higher level (ZnSe) to the other lower levels. Therefore, the Fermi level of ZnSe would shift down with respect to the location of Fermi level in TiO_2, and the conduction band edges of CdS and CdSe are elevated. Such electron transfer is known as the Fermi level alignment.[20] The photoexcited electrons would transfer from the higher conduction band to the lower band with the help of a driving force. Therefore, the resulting conduction band edges for the ZnSe/CdS/CdSe device are inferred to have a stepwise structure, as shown in Fig. 8b. Both the conduction and valence band edges of the three materials increase in the order: TiO_2 < ZnSe < CdS < CdSe, which is advantageous not only for electron injection, but also for hole recovery for all three layers. The layer of ZnSe also acts as a blocking layer to shield the TiO_2 core from the outer CdS/CdSe QDs and electrolyte, and provides a physical separation of the injected electrons in TiO_2 from the positively charged QDs and the electrolyte, thus retarding the interfacial recombination to obtain a high V_{OC}. This inference is sustained by the *I–V* characteristics measured under dark conditions (shown in Fig. S3†), which presents the smallest dark current for the cell with the TiO_2/ZnSe/CdS/CdSe photoelectrode. Therefore, this photoelectrode contributes an interfacial structure with superior ability in collecting the excited electrons and retarding the recombination of excited electrons at the electrode/electrolyte interface.[33]

On the contrary, in the case of TiO_2/CdSe/CdS/ZnSe, the Fermi level alignment results in notable barriers for injecting an excited electron from the outer ZnSe layer and for transferring a hole out of inner CdSe, as shown in Fig. S4.† The photoexcited electrons (holes) can transfer smoothly from CdSe (TiO_2) to TiO_2 (CdSe); however, the electrons (holes) excited in CdS or ZnSe (TiO_2) cannot transfer effectively to TiO_2 (CdS or ZnSe). Instead, some of the photoexcited electrons (hole) in

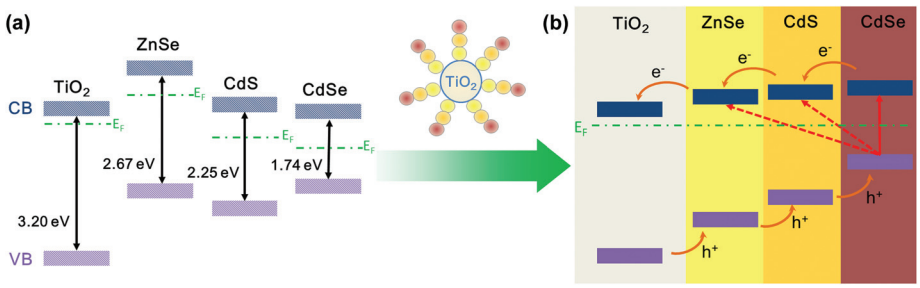

Fig. 8 (a) Relative band positions of TiO_2, ZnSe, CdS, and CdSe in bulk and (b) ideal stepwise structure of band edges for the efficient transport of excited electrons and holes in a TiO_2/ZnSe/CdS/CdSe photoelectrode.

CdSe/CdS (CdS/ZnSe) are transferred to CdS/ZnSe (CdSe/CdS).[31,34] Thus, the blocked photoexcited electrons and holes increase the charge recombination loss and decrease the photocurrent (Fig. S5†), leading to very low efficiency. A comparison of the *I–V* performance between TiO_2/ZnSe/CdS/CdSe and TiO_2/CdSe/CdS/ZnSe clearly supports the occurrence of band alignment between these QDs. This suggests that excited electrons in the former (with cascade band alignment) can more efficiently inject than those in the latter (without alignment), which supports the previous direct evidence[35] that both the conduction band edge and valance band edge are located at a higher energy level with respect to that of TiO_2, constructing a stepwise structure of the band-edge levels in the TiO_2/CdS/CdSe electrode. These results show that the deposition order of the layers is also responsible for the performance of multilayered QD-sensitized solar cells.

Conclusions

In this study, the model sensitizer of three semiconductor QDs layers, ZnSe/CdS/CdSe, was successively prepared by a series of SILAR procedures in a reproducible and controllable manner, and further demonstrated to be promising photoelectrodes for QDSSCs. EDX composition mapping confirms the presence and homogeneous distribution of elemental cadmium, selenium, zinc, and sulfur with different atomic ratios. The absorbance increases with the increasing number of SILAR cycles, indicating an increased adsorption of QDs. Furthermore, the red shift of the absorption shoulder with the increasing number of SILAR cycles implies the growth of QDs. The pre-assembled ZnSe QD layer could act as a seed layer to facilitate the nucleation of CdS, and thus the amount of CdS deposited is larger than that achieved for deposition on bare TiO_2 films. CdS and CdSe QDs have a complementary effect on the light harvesting. The performance of the devices is dependent on the number of SILAR cycles for assembling the CdSe QDs. Overloading of the CdSe QDs on a TiO_2 film was reported to be disadvantageous to the cell performance, due to the blocking of the mesopores by the additional loading of CdSe. The device with TiO_2/CdS generated a η of 1.09%, whereas that with TiO_2/ZnSe/CdS generated a η of 2.07%. As a result, the overall power conversion efficiency increases noticeably after introducing the CdSe layer, and a maximum value as high as 4.94% was obtained at six SILAR cycles. According to the EIS results, the most appropriate layered structure for the SILAR process should be TiO_2/ZnSe(10)/CdS(5)/CdSe(6), which provides the longest electron lifetime. The long-lived charge carrier implies low charge recombination to improve the V_{oc} and FF of QDSSCs. For the TiO_2/ZnSe/CdS/CdSe electrode, the re-organization of the energy levels among ZnSe, CdS and CdSe forms a stepwise structure of band-edge levels, which is potentially more favorable for the transport of both electrons and holes across the photoelectrode. In addition, this photoelectrode contributes an interfacial structure that inhibits charge recombination at the electrode/electrolyte interface, thus yielding a higher efficiency of QDSSCs based on TiO_2/ZnSe/CdS/CdSe. In contrast, the reverse structure (TiO_2/CdSe/CdS/ZnSe) would induce a significant recombination of electrons and holes. In conclusion, J_{SC} and η of QDSSCs based on multilayered QD-sensitizers are mainly influenced by two factors: (1) light absorption intensity determined by both the material and the amount of QD; and (2) electron transport influenced by the position of the band edge and deposition order of the layers.

Acknowledgements

This work was supported in part by the National Science Foundation (DMR 1035196), University of Washington TGIF grant, Royalty Research Fund (RRF) from the Office of Research at University of Washington. Part of this work was conducted at the University of Washington NanoTech User Facility, a member of the NSF National Nanotechnology Infrastructure Network (NNIN). The authors wish to thank China Scholarship Council (CSC) for its fellowship assistance.

References

1 K. Hara, Z. S. Wang, T. Sato, A. Furube, R. Katoh, H. Sugihara, Y. Dan-oh, C. Kasada, A. Shinpo and S. Suga, *J. Phys. Chem. B*, 2005, **109**, 15476–15482.
2 C. Sealy, *Nano Energy*, 2012, **1**, 1–2.
3 P. Poudel, A. Thapa, H. Elbohy and Q. Qiao, *Nano Energy*, 2014, **5**, 116–121.
4 E. Lee, C. Kim and J. Jang, *Chem. – Eur. J.*, 2013, **19**, 10280–10286.
5 C.-T. Wu, W.-P. Liao and M. Yoshimura, *Nano Energy*, 2013, **2**, 1354–1372.
6 M. M. Lee, J. Teuscher, T. Miyasaka, T. N. Murakami and H. J. Snaith, *Science*, 2012, **338**, 643–647.
7 G. E. Eperon, V. M. Burlakov, P. Docampo, A. Goriely and H. J. Snaith, *Adv. Funct. Mater.*, 2014, **24**, 151–157.
8 W. W. Yu, L. H. Qu, W. Z. Guo and X. G. Peng, *Chem. Mater.*, 2003, **15**, 2854–2860.
9 H. Tada, M. Fujishima and H. Kobayashi, *Chem. Soc. Rev.*, 2011, **40**, 4232–4243.
10 Y. R. Smith and V. Subramanian, *J. Phys. Chem. C*, 2011, **115**, 8376–8385.
11 P. K. Santra and P. V. Kamat, *J. Am. Chem. Soc.*, 2012, **134**, 2508–2511.
12 S. Bayram and L. Halaoui, *Part. Part. Syst. Charact.*, 2013, **30**, 706–714.
13 F. Liu, J. Zhu, J. F. Wei, Y. Li, L. H. Hu, Y. Huang, Q. Takuya, Q. Shen, T. Tpyoda, B. Zhang, J. X. Yao and S. Y. Dai, *J. Phys. Chem. C*, 2014, **118**, 214–222.
14 J. A. Seabold, K. Shankar, R. H. T. Wilke, M. Paulose, O. K. Varghese, C. A. Grimes and K.-S. Choi, *Chem. Mater.*, 2008, **20**, 5266–5273.
15 Z. Tachan, M. Shalom, I. Hod, S. Rühle, S. Tirosh and A. Zaban, *J. Phys. Chem. C*, 2011, **115**, 6162–6166.

16 H. Wang, T. Kubo, J. Nakazaki, T. Kinoshita and H. Segawa, *J. Phys. Chem. Lett.*, 2013, **4**, 2455–2460.
17 W. K. Bae, J. Joo, L. A. Padilha, J. Won, D. C. Lee, Q. Lin, W. Koh, H. Luo, V. I. Klimov and J. M. Pietryga, *J. Am. Chem. Soc.*, 2012, **134**, 20160–20168.
18 Y. Cui, J. Wang, S. R. Plissard, A. Cavalli, T. T. T. Vu, R. P. J. Veldhoven, L. Gao, M. Trainor, M. A. Verheijen, J. E. M. Haverkort and E. P. A. M. Bakkers, *Nano Lett.*, 2013, **13**, 4113–4117.
19 X. F. Gao, W. T. Sun, G. Ai and L. M. Peng, *Appl. Phys. Lett.*, 2010, **96**, 153104.
20 Y.-L. Lee and Y.-S. Lo, *Adv. Funct. Mater.*, 2009, **19**, 604–609.
21 H. J. Lee, J. Bang, J. Park, S. Kim and S.-M. Park, *Chem. Mater.*, 2010, **22**, 5636–5643.
22 J. J. Tian, R. Gao, Q. F. Zhang, S. G. Zhang, Y. W. Li, J. Lan, X. H. Qu and G. Z. Cao, *J. Phys. Chem. C*, 2012, **116**, 18655–18662.
23 L. Yang, R. Zhou, J. Lan, Q. F. Zhang, G. Z. Cao and J. G. Zhu, *J. Mater. Chem. A*, 2014, **2**, 3669–3676.
24 J. Zhang, M. J. Li, Z. C. Feng, J. Chen and C. Li, *J. Phys. Chem. B*, 2006, **110**, 927–935.
25 Y.-L. Lee, B.-M. Huang and H.-T. Chien, *Chem. Mater.*, 2008, **20**, 6903–6905.
26 X. Y. Yu, J. Y. Liao, K. Q. Qiu, D. B. Kuang and C. Y. Su, *ACS Nano*, 2011, **5**, 9494–9500.
27 I. Mora-Seró, S. Giménez, F. Fabregat-Santiago, R. Gómez, Q. Shen, T. Toyoda and J. Bisquert, *Acc. Chem. Res.*, 2009, **42**, 1848–1857.
28 J. Xu, X. Yang, Q.-D. Yang, T.-L. Wong and C.-S. Lee, *J. Phys. Chem. C*, 2012, **116**, 19718–19723.
29 M. Grätzel, *Nature*, 2001, **414**, 338–344.
30 X. H. Zhong, R. G. Xie, Y. Zhang, T. Basché and W. Knoll, *Chem. Mater.*, 2005, **17**, 4038–4042.
31 Y.-L. Lee, C.-F. Chi and S.-Y. Liau, *Chem. Mater.*, 2010, **22**, 922–927.
32 B.-R. Hyun, Y.-W. Zhong, A. C. Bartnik, L. F. Sun, H. D. Abruña, F. W. Wise, J. D. Goodreau, J. R. Matthews, T. M. Leslie and N. F. Borrelli, *ACS Nano*, 2008, **2**, 2206–2212.
33 J. Xu, X. Yang, Q. D. Yang, T. L. Wong, S.-T. Lee, W. J. Zhang and C.-S. Lee, *J. Mater. Chem.*, 2012, **22**, 13374–13379.
34 M. Seol, H. Kim, W. Kim and K. Yong, *Electrochem. Commun.*, 2010, **12**, 1416–1418.
35 C. F. Chi, H. W. Cho, H. Teng, C. Y. Chuang, Y. M. Chang, Y. J. Hsu and Y. L. Lee, *Appl. Phys. Lett.*, 2011, **98**, 012101.

